Journal of Food Engineering 340 (2023) 111308

Contents lists available at ScienceDirect

Journal of Food Engineering

journal homepage: www.elsevier.com/locate/jfoodeng

Experimental and simulation-based investigation of the interplay between factor gradients following pulsed electric field treatments triggering whey protein aggregation

Robert D. Axelrod [a,b], Julia Baumgartner [a], Michael Beyrer [b,*], Alexander Mathys [a]

[a] ETH Zurich, Laboratory of Sustainable Food Processing, Institute of Food, Nutrition and Health, Schmelzbergstrasse 9, 8092, Zürich, Switzerland
[b] University of Applied Sciences and Arts Western Switzerland Valais-Wallis (HES-SO VS), Institute of Life Technologies, Food Engineering Group, Rue de l'Industrie 19, 1950, Sion, Switzerland

ARTICLE INFO

Keywords:
Pulsed electric field
Factor gradients
Whey proteins
Simulation
Process control

ABSTRACT

Novel pulsed electric field (PEF) applications to modify the techno-functionality of biomacromolecules have recently emerged. Insights into the involved interplay of factor domains (electrical, flow, concentration, temperature) with respect to the treatment chamber locations, and into the scalability are lacking. Therefore, a parallel plate batch (0.8 mL) and a scaled up parallel plate continuous (50 mL, 0.83 mL s^{-1}) setup were built and simulated to investigate these domains and resulting gradient interactions using liquid whey protein solutions (0.5% w/w). In both setups, protein agglomerations and aggregations were observed below 60 °C at the electrode boundary layers for pulses in the range of 2–2.5 kV cm^{-1}, 10 μs, 40–350 Hz. The boundary layer is characterized by higher protein concentrations due to temperature- and pH-dependent migration trajectories, increased electrochemical reactivity (e.g., pH), and increased residence times due to the laminar flow or no flow conditions. Characterizing the domain interconnectivity led to effective scaling-up approaches of protein aggregations and insights into involved mechanisms.

1. Introduction

Pulsed electric field (PEF) technology is a versatile electromagnetic processing method that has a great potential in the food- and biobased industry (Buchmann and Mathys, 2019; Rocha et al., 2018). Changing the treatment parameters (e.g., electric field intensity, pulse length, pulse repetition frequency) results in an altered process window and thus leads to different treatment effects, such as facilitated extraction of compounds, microbial inactivation, growth stimulation, or protein structural changes (Buchmann et al., 2019; Canelli et al., 2022; Giteru et al., 2018; Knirsch et al., 2010). The ensuing effects are dependent on a shift in dominance of occurring mechanisms during PEF treatment: electroporation, ohmic heating, cathodic and anodic reactions, protonation and deprotonation, and electrophoretic mobility (Fritsch and Krause, 2003; Meneses et al., 2011a; Zimmermann et al., 1974). To successfully achieve the desired effect(s) in a given matrix, a precise characterization and a complete control of the PEF treatment geometry (e.g., parallel plate, co-linear, co-axial), generator system (e.g., voltage, pulse length, pulse shape), and substrate parameters (e.g., temperature, conductivity, viscosity) is essential (Raso et al., 2016).

Multiphysics simulations overlay flow fields in continuous systems with electric fields and temperature fields, providing additional insights into physical processes occurring during PEF treatments. In previous studies, simulations included the analysis of fluid flow and ohmic heating to improve the uniformity of the electric field, to minimize the risk of the dielectric breakdown, and to reduce the occurrence of temperature hot spots (Gerlach et al., 2008; Lindgren et al., 2002). The design of co-linear PEF treatment chambers was further optimized by simulating the insertion of grids into the flow channel to trigger an increase of turbulence, thereby increasing the microbial decontamination efficiency while simultaneously decreasing the impact on alkaline phosphatase activity (Jaeger et al., 2009). Another approach to reduce temperature peaks and the overall thermal load of a co-linear treatment chamber was to simulate the active cooling of the electrodes with a jacketed heat-exchanger (Meneses et al., 2011b). Simulations in a co-linear treatment chamber further helped predict the turbulent flow pattern, electric field distribution, temperature increase and residence time in a scaled up setup (Buckow et al., 2010). In a second step, the

* Corresponding author.
E-mail address: michael.beyrer@hevs.ch (M. Beyrer).

https://doi.org/10.1016/j.jfoodeng.2022.111308
Received 15 June 2022; Received in revised form 14 September 2022; Accepted 28 September 2022
Available online 10 October 2022

treatment chamber was optimized with an iterative algorithm (Knoerzer et al., 2012). Since the pH influences the microbial inactivation during PEF treatments, locally occurring pH shifts were investigated and shifts of up to a value of 4.04 were predicted by simulations based on the finite element method and validated in a batch parallel plate setup (Meneses et al., 2011a). To control the PEF system, it is furthermore of importance to gain an understanding of the electrode degradation and metal release phenomena. A validated model for the spatial distribution of metallic elements as a function of the electric field strength, specific energy input, and medium composition in a continuous parallel plate at 25 °C was generated and simulated (Pataro et al., 2015).

Simulations done in previous studies thus far lack to characterize the overlapping physical fields and to bring their effects into the context of targeted protein modifications. For instance, it was reported that PEF treatments in the microsecond range (μsPEF) resulted in the formation of whey protein aggregates and agglomerates near the anode at time-temperature profiles for which no aggregates were detected under purely thermal treatment conditions (Axelrod et al., 2022). It remains unclear which effects and local gradients are responsible for the observed protein layer formation.

Therefore, the aim of this study was to shed light upon the field and gradient distributions in parallel plate treatment geometries, to visualize idealized protein monomer migration trajectories, and to translate the findings from a batch (0.8 mL) to a scaled up continuous (50 mL) setup using reconstituted whey protein concentrate (WPC_L) as a model fluid and validation tool.

2. Materials and methods

Symbols used in the equations and found in the text to describe relevant parameters are presented and summarized in Table 1.

Table 1
List of symbols.

	SI Unit	Definition
Latin letters		
c_p	J kg^{-1} K^{-1}	Specific heat capacity
D	mol m^{-2} s^{-1}	Diffusion flux
E	V m^{-1}	Electric field intensity | Electric field strength
f	Hz	Pulse repetition frequency
F_d	N	Stokes' drag
F_{DL}	N	Double layer forces
F_{el}	N	Electric forces
F_{ext}	N	External forces
F_{flow}	N	Flow forces
F_{VdW}	N	Van der Waals forces
I	A	Electric current
J	A m^{-2}	Current density
K	W m^{-1} K^{-1}	Thermal conductivity
m	kg	Mass of the fluid treated in the treatment chamber
m_p	kg	Mass of the particle (trajectory simulation)
p	Pa	Pressure
Q	J kg^{-1}	Heat source or sink
q	C	Electric charge
r_p	m	Radius of the particle
T	K	Temperature
t	s	Time of process | Simulation time
t_{PEF}	s	μsPEF treatment time
t_r	s	Residence time
U	V	Electric potential difference | voltage
V	m s^{-1}	Velocity
W_s	J kg^{-1}	Specific energy input
Greek letters		
η	Pa s	Dynamic viscosity
ρ	kg m^{-3}	Density
ρ_c	C m^{-3}	Charge density
σ	S m^{-1}	Electrical conductivity
τ_{pulse}	s	Pulse length

2.1. Reconstituted whey protein concentrate

The preparation and whey protein composition is described in detail elsewhere (Axelrod et al., 2021). Briefly, spray-dried whey protein concentrate powder was kindly provided by Hochdorf Swiss Nutrition AG, Switzerland, and reconstituted in ultrapure water (18.2 MΩ cm, 25 °C) at a concentration of 0.5% w/w (0.4% w/w protein concentration), ensuring a controllable system. The reconstituted liquid (WPC_L) was stirred for 30 min, placed into the refrigerator overnight at 4 °C, heated up to 55 °C to increase the protein solubility and cooled down to room temperature before usage. The $pH_{25°C}$ (6.8, 5.3 and 3.8) and electrical conductivity (136 μS cm^{-1}, 235 μS cm^{-1}, 237 μS cm^{-1}, 424 μS cm^{-1}) values of WPC_L were adjusted with HCl (1 M) or NaCl (1 M).

2.2. Pulsed electric field and purely thermal treatments

Both the batch and the continuous treatment chambers were connected to a RUP6-15CL pulse generator (GBS-Elektronik GmbH, Radeberg, Germany) and an external trigger (15 MHz FG300, Yokogawa Electric, Musashino, Tokyo, Japan). The unipolar square-wave pulses (Fig. S1) were quantified using a voltage probe (P6015A, Tektronix Inc., Beaverton, OR, USA), a current monitor (Model 110, Pearson Electronics Inc., Palo Alto, CA, USA) and an oscilloscope (Wave Surfer 10, Teledyne LeCroy GmbH, Heidelberg, Germany). The specific energy input W_s (J kg^{-1}) during the time of process t (batch) or residence time $t_r = \frac{Treatment\ chamber\ volume}{Volume\ flow\ rate}$ (continuous) was calculated according to Eq. (1) (Raso et al., 2016).

$$W_s = \frac{1}{m}\int_0^t U(t)\cdot I(t)dt \quad (1)$$

Parameter m (kg) denotes the mass of WPC_L treated in the PEF treatment chamber during the time of process or residence time, U (V) the electric potential difference, and I (A) the electric current.

An in depth description of linking the specific energy input to the observed temperature increase and differentiating time of process from pulsed electric field treatment times (t_{PEF}) have been published recently (Axelrod et al., 2022).

2.2.1. Pulsed electric field in a batch setup

Microsecond pulsed electric field (μsPEF) treatments of WPC_L were conducted in electroporation cuvettes (Z706094, Sigma-Aldrich, St. Louis, Missouri, USA) and are described in detail in published work (Axelrod et al., 2022). In summary, the treatment volume (V) was 0.8 mL, the electrodes made from stainless steel with a distance (d) of 0.4 cm. The electric field intensity (E), pulse length (τ_{pulse}), and pulse repetition frequency (f) were kept constant (2.5 kV cm^{-1}, 10 μs, 40 Hz) for all WPC_L with varying pH and electrical conductivity values. Pulses were applied during 20 min and the temperature measured with a fiber-optic sensor (TS4, Weidmann Technologies Deutschland GmbH, Dresden, Germany).

2.2.2. Pulsed electric field in a continuous setup

Continuous μsPEF treatments were conducted in a polycarbonate-based treatment chamber (designed and manufactured at HES-SO VS, Switzerland) with stainless steel electrodes and a diffuser inlet/outlet (constant cross-sectional area) (Fig. 1). The electrodes had a surface area of 100 cm^2 and were separated by a gap of 0.5 cm. Keeping the peak plateau voltage constant at a value of around −1 kV, E resulted in a value of 2 kV cm^{-1} (Fig. S1). To achieve similar and slightly higher time-temperature profiles than in the batch system, τ_{pulse} was chosen at 10 μs and f between 250 Hz and 350 Hz. WPC_L was pumped through silicone tubes (d = 0.7 cm) into the treatment chamber from the bottom to the top with a gear pump (MCP-Z Standard, ISMATEC®, Cole-Parmer GmbH, Wertheim, Germany) at a flow rate of 0.83 mL s^{-1}. The temperature was quantified with a K-Type thermocouple (TES Electrical

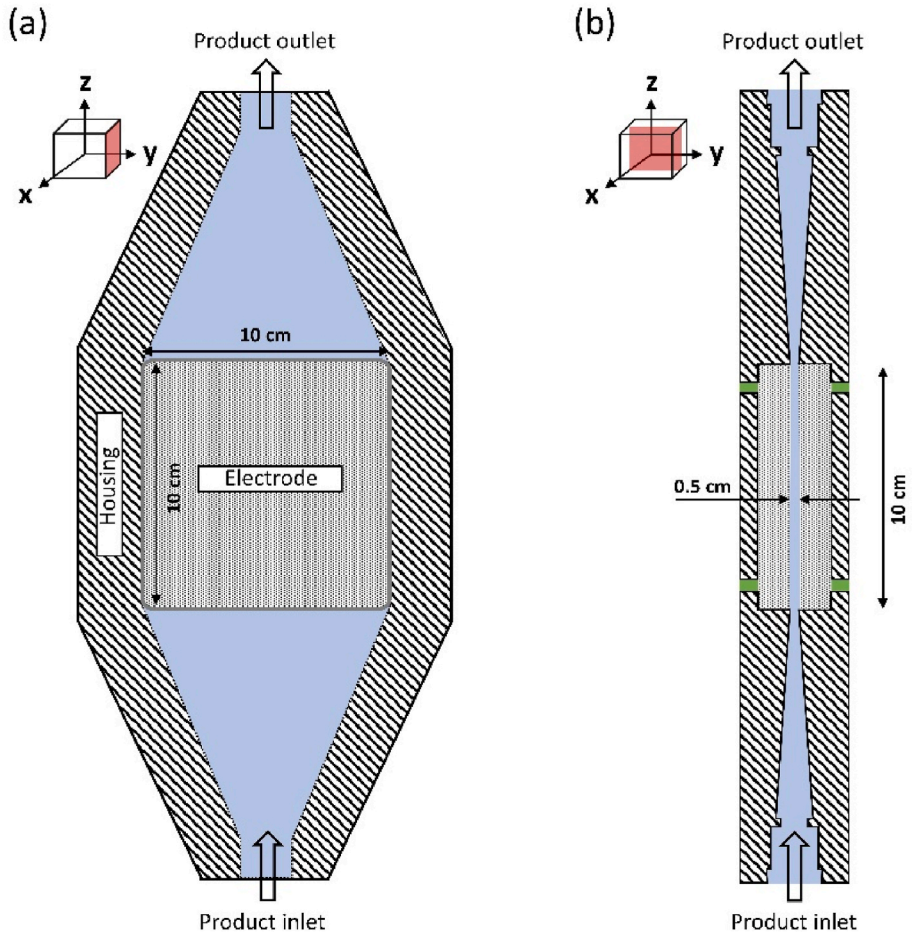

Fig. 1. Schematic drawings in the (a) x-z-plane and in the (b) y-z-plane of the continuous treatment chamber with a diffuser inlet/outlet (constant cross-sectional area) and square electrodes in the center. The three-dimensional cubes are intended to increase the readability and interpretation of graphs. Hollow arrows represent the fluid flow direction, i.e., from bottom to top allowing air bubbles to escape more easily. Striped areas represent the housing and dotted areas correspond to the electrodes. Treatment volume = 50 mL and electrode distance = 0.5 cm.

Electronic Corp., Taipei, Taiwan) at the outlet.

2.2.3. Purely thermal treatments

Electroporation cuvettes were filled with WPC_L and submerged in a water bath set to 66 °C for 20 min. This temperature choice allowed a comparison to similar temperatures reached by means of μsPEF treatments. The change in temperature was measured with a fiber optic sensor.

2.3. Total nitrogen (TN) content measurements

To estimate the amount of whey proteins involved in aggregate formation and air-liquid interface adsorption, treated and untreated WPC_L was left to undergo gravitational sedimentation during 5 h at room temperature. The supernatant was collected, diluted by a factor of 75 and analyzed by a TOC-L connected to a TN module (Shimadzu Europa, Duisburg, Germany).

2.4. Simulations

2.4.1. Multiphysics simulation

Electroporation cuvette and continuous diffuser inlet/outlet treatment chambers were recreated as 3D models in COMSOL Multiphysics® (version 6.0, Comsol Inc., Burlington, MA, USA). With a calculated Reynolds number of around 90 at 20 °C for the tube inlet, laminar flow was assumed to be fully established and thus, a laminar flow approach was implemented for the continuous setup. The rectangular pulses were incorporated in the simulation by multiplying the total power dissipation density by τ_{pulse} and f (Buckow et al., 2012). Due to the low dry solid content of WPC_L (0.5% w/w), the model fluid was assumed to be water-like with higher electrical conductivity values. The electrical conductivity as a function of temperature was calculated based on voltage and electric current measurements. Input parameters and study conditions for batch and continuous simulations can be found in Table S.1 and Table S.2, respectively. The mesh consisted of free tetrahedrons and was calibrated for fluid dynamics. The mesh number, the mesh size, the sensitivity analysis and the element quality analysis for the selected mesh are shown in Fig. S2 and Fig. S3. The boundary conditions included no wall slip, atmospheric pressure, thermal insulation, resistance heating, natural convection, convective heat transfer, radiation, voltage source, ground, and electrical insulation. The interplay between fluid flow, electric current, and heat transfer were governed by the conservation of mass, momentum, charge, and energy (Gerlach et al., 2008; Jaeger et al., 2009; Meneses et al., 2011a). The governing equation for the momentum balance from the Navier-Stokes equations, assuming an incompressible fluid and laminar flow, is shown in Eq. (2), where ρ (kg m^{-3}) represents the density, v (m s^{-1}) the velocity, p (Pa) the pressure, η (Pa·s) the dynamic viscosity, F_{ext} (N) external forces, and t (s) time. T and ∇ correspond to the transpose and Nabla-operator, respectively.

$$\rho\left(\frac{\delta v}{\delta t}+(v \bullet \nabla)v\right) = -\nabla p+\nabla \bullet \left(\eta(\nabla v+(\nabla v)^{T})\right)+F_{ext} \quad (2)$$

The governing equation for the charge conservation is given by the continuity equation (Eq. (3)), where J (A m^{-2}) represents the current density and ρ_c (C m^{-3}) the charge density.

$$\nabla \bullet J+\frac{\delta \rho_c}{\delta t}=0 \quad (3)$$

The governing equation for the heat transfer is stated in Eq. (4),

where Q (J kg^{-1}) represents the heat source or sink, c_p (J kg^{-1} K^{-1}) the specific heat capacity, T (K) the temperature, and k (W m^{-1} K^{-1}) the thermal conductivity.

$$Q = \rho \bullet c_p(T) \bullet \frac{\delta T}{\delta t} + \rho \bullet c_p(T) \bullet v \bullet \nabla T + \nabla \bullet (-k(T) \bullet \nabla T) \quad (4)$$

When the resistive heating caused by the μsPEF application is considered, the energy equation is coupled with the current density J and the electric field intensity E (V m^{-1}) (Eq. (5)).

$$\nabla \bullet (k(T) \bullet \nabla T) + J \bullet E = \rho \bullet c_p(T) \bullet \frac{\delta T}{\delta t} + \rho \bullet c_p(T) \bullet v \bullet \nabla T \quad (5)$$

To validate the simulations, the temperature (point) in the middle of the geometry (batch setup) and at the outlet (continuous setup) were compared to experimentally measured values.

2.4.2. Migration simulation

To gain an insight into the potential trajectory of β-lactoglobulin (β-lg) and calcium ions (Ca^{2+}) contributing to a concentration gradient, simulations written in Python were implemented. The simulated flow field of the multiphysics simulations were incorporated, however, the simulations were not coupled. The used scripts providing further input data, including the values for the parameters in Eqs. (6)–(8), can be found in the supplementary information.

In the batch and continuous setup, the following assumptions were made for an idealized system. The size and weight of β-lg corresponded to that of a monomer, despite the presence of dimers below 40 °C and smaller aggregates from spray drying (Axelrod et al., 2022; Tolkach and Kulozik, 2007). Simulations neglected protein bounded ions, charge screening, and the concentration-based diffusion flux from the boundary layer back into the bulk. Lastly, migration simulations were only conducted with one molecule or ion at a time in 2D, i.e., interactions with other particles were not taken into account. In the positive and negative direction of the electric field (distance from the center of the treatment chamber, y), the trajectory of a particle was assumed to be governed by the electric force F_{el} and Stokes' drag F_d during the simulation time duration t (s) (Eq. (6)).

$$m_p \bullet \frac{d^2y}{dt^2} = F_{el} - F_d \quad (6)$$

To describe the two forces (F_{el} and F_d), the electric charge q (C), the electric field intensity E (V m^{-1}), the temperature T (K) dependent viscosity η (Pa·s), the radius r_p (m), and the mass of the particle m_p (kg) are considered. The electric force F_{el} is substituted with $q \bullet E$ and the Stokes' drag force F_d with $6\pi \bullet \eta(T) \cdot r_p \cdot \frac{dy}{dt}$ (Eq. (7)).

$$\frac{d^2y}{dt^2} = \frac{q \bullet E - 6\pi \bullet \eta(T) \cdot r_p \cdot \frac{dy}{dt}}{m_p} \quad (7)$$

The analytical solution of the second order differential equation, shown here for the initial conditions y (0) = 0 and ẏ(0) = 0, was implemented for the particle trajectory in the positive and negative direction of the electric field (Eq. (8)).

$$y(t) = \frac{\frac{q \bullet E}{m_p}\left(-1 + e^{-\frac{6\pi \bullet \eta(T) \cdot r_p}{m_p} \bullet t} + \frac{6\pi \bullet \eta(T) \cdot r_p}{m_p} \bullet t\right)}{\left(\frac{6\pi \bullet \eta(T) \cdot r_p}{m_p}\right)^2} \quad (8)$$

In the batch setup, the movement along the treatment chamber length (z) was assumed to be equal to 0 during a simulation time of 60 s and temperatures to determine the viscosity were selected for the highest temperature at 20 min to determine the maximal effects of the temperature. For the migration simulations, the starting y/z-coordinates were chosen for (−0.0015/0.005), (−0.001/0.0075), (0/0.01), (0.0015/0.015). The simulated pulse corresponded to a 2.5 kV cm^{-1}, 10 μs, 40 Hz μsPEF treatment. In the continuous setup, in direction from the inlet to the outlet (treatment chamber length, z), a parabolic function representing the laminar flow profile and a temperature gradient resulting from the time-dependent multiphysics simulations were implemented (Fig. S4). For β-lg in the continuous setup, the coordinates (−0.0017/0), (−0.0015/0), (−0.0013/0), (−0.001/0), (−0.0007), (0/0), (0.0007/0), (0.0015/0), (0.0025/0) were selected and for Ca^{2+}, the starting positions (−0.0025/0), (−0.002/0), (−0.001/0), (0/0), (0.0015/0). The simulated pulse corresponded to a 2 kV cm^{-1}, 10 μs, 300 Hz μsPEF treatment.

2.5. Software

Graphs were plotted in Origin (2019) (OriginLab Corporation, Northhampton, MA, USA). The Chimera package and the 1B0O protein data bank file were used to generate the β-lg monomers (Pettersen et al., 2004; Wu et al., 1999). Visualizations were created in Affinity Designer (version 1.10, Serif Ltd, West Bridgford, UK), Blender (version 2.8, Blender Foundation, Amsterdam, Netherland), and PowerPoint® (version 2108, Microsoft Corporation, Redmond, WA, USA). Multiphysics simulations were done in COMSOL Multiphysics® (version 6.0, Comsol Inc., Burlington, MA, USA), particle trajectory simulations were written in Python (version 3.7.0, Python Software Foundation, Wilmington, DE, USA), and differential equation solving in Wolfram Mathematica (version 11, Champaign, IL, USA).

3. Results and discussion

3.1. Interplay between factor domains in batch

The time-temperature profiles and average equilibrium temperatures resulting from identical microsecond pulsed electric field (μsPEF) parameter settings (2.5 kV cm^{-1}, 10 μs, 40 Hz) varied due to an increase in the electrical conductivity following HCl addition in order to lower the pH of liquid whey protein concentrate (WPC_L) (Fig. 2a). Increasing the conductivity from 136 μS cm^{-1} to 424 μS cm^{-1} increased the energy input from 540 ± 188 J g^{-1} to 1648 ± 229 J g^{-1} during a time of process of 20 min, resulting in higher (ΔT = 26.07 ± 1.7 °C) average equilibrium temperatures. The interconnectivity and interdependency of the involved generator, treatment chamber, and medium parameters has been qualitatively well described and established (Jaeger and Knorr, 2017). The addition of NaCl instead of HCl to WPC_L increased the conductivity by the same amount without lowering the pH and led to a comparable time-temperature profile and to similar equilibrium temperatures. The total nitrogen (TN) content after sedimentation dropped by a factor of 2.32 ± 0.46 when comparing WPC_L with the lowest conductivity at 136 μS cm^{-1} to WPC_L with the highest conductivity at 424 μS cm^{-1} (Fig. 2b). The drop in TN can be linked to aggregates and agglomerates forming at the electrodes and potentially to a stabilizing activity at the interface of forming gas bubbles from electrolysis (Fig. 3, Fig. S5). Higher ion concentrations led to more gas evolution. The increased formation of gas bubbles at higher ion concentrations can be controlled and reduced with shorter pulse durations or bipolar pulses (Samaranayake et al., 2005; Timmermans et al., 2019). It is noteworthy that $pH_{25°C}$ values at 6.8 and 5.3 led to a protein layer at the anode (ground), while a value of 3.8 led to a layer forming at the cathode (negative high voltage). Adding NaCl instead of HCl to WPC_L, resulting in similar electrical conductivities, led to a comparable TN reduction. Purely thermal treatments (indirect conductive heat transfer) at the lowest tested pH of 3.8 resulted in no TN reduction despite being exposed to higher temperatures at every time-point during a time of process of 20 min.

The most abundant protein in WPC_L is β-lg (Whitney et al., 1976). The isoelectric point of β-lg is between 5.1 and 5.3. At higher pH values the net charge of β-lg is negative, and at lower pH values the net charge is positive (Engelhardt et al., 2013). Consequently, negatively charged proteins migrate towards the positively charged electrode and vice versa. Migration simulations for β-lg monomers during 60 s in an

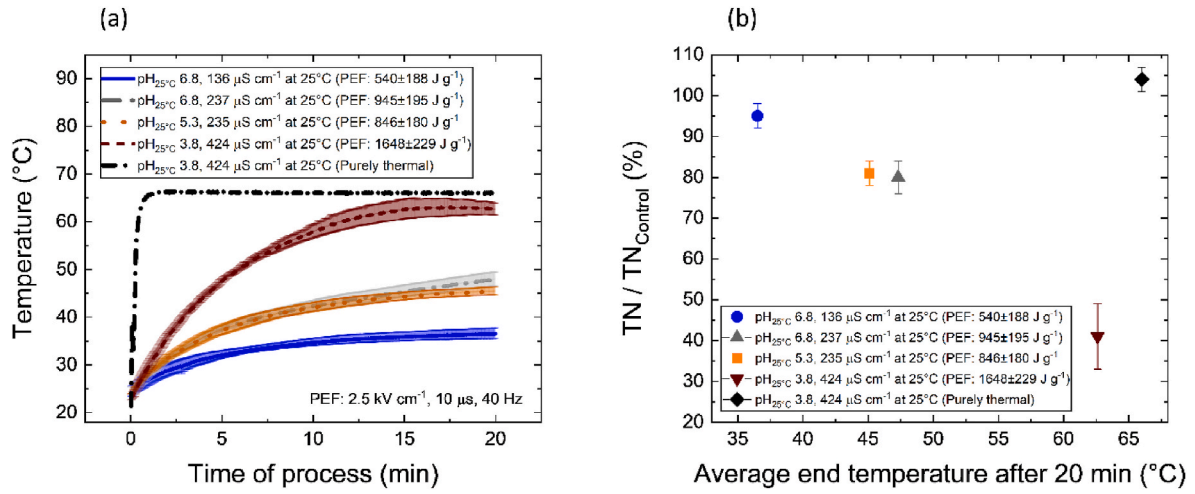

Fig. 2. (a) Time-temperature profiles resulting from purely thermal treatments (no ohmic heating) or from pulsed electric field (PEF) treatments (2.5 kV cm^{-1}, 10 µs, 40 Hz) of reconstituted liquid whey protein concentrate (WPC_L, 0.5% w/w) with different pH values in electroporation cuvettes (0.8 mL). (b) Total nitrogen (TN) content of WPC_L measured after PEF and purely thermal treatments normalized by the control (untreated WPC_L). Error bars represent the standard deviation (n = 3).

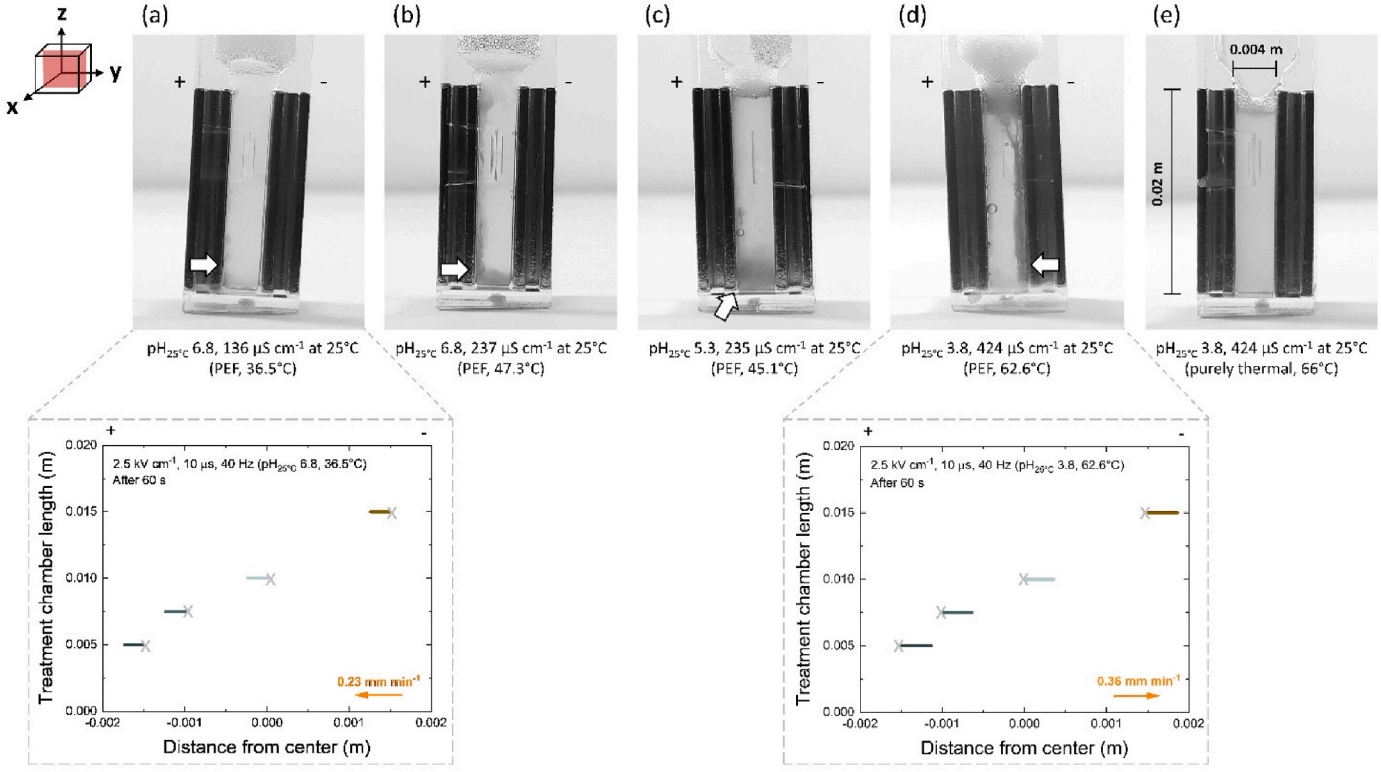

Fig. 3. Reconstituted liquid whey protein concentrate (WPC_L, 0.5% w/w) after (a–d) PEF treatments (2.5 kV cm^{-1}, 10 µs, 40 Hz) at different pH values and (e) a purely thermal treatment in electroporation cuvettes (0.8 mL). Temperatures in brackets relate to the measured end temperature of the treatment. White arrows indicate where protein layers were observed. Graphs for (a) and (d) represent the coordinate system of the cuvette and show migration simulations of a β-lg monomer in between the electrodes during 60 s at different starting positions (indicated by the X). The migration direction and velocity are indicated by the arrow and is influenced by the pH (charge of β-lg), temperature, and applied pulse parameters. Plus and minus symbols above the 1st and 2nd y-axis represent the ground and high voltage electrodes, respectively. The three-dimensional cube is intended to increase the readability and interpretation, i.e., which plane the data is plotted in.

idealized matrix and system reinforced this observation that the migration direction inverses (Fig. 3a and d). The calculated migration velocity of 0.23 mm min^{-1} at a $pH_{25°C}$ of 6.8 and a migration velocity of 0.36 mm min^{-1} at a $pH_{25°C}$ of 3.8 was dependent on the temperature (Eq. (8)). Since higher average equilibrium temperatures were reached at higher conductivities and were considered in the simulations, a faster protein migration velocity was predicted. It is assumed that the calculated values are at their absolute maximum, since the velocity would decrease substantially if larger particles (dimers or aggregates), protein interactions, and charge shielding phenomena had been additionally considered.

A multiphysics simulation for WPC_L at a $pH_{25°C}$ value of 6.8 and 5.3 further deepened the understanding of the interplay between factor domains within the batch treatment chamber. In the simulation, the

temperature increase as a function of time was comparable to the experimental data (Fig. 4a, Fig. 4b). The difference between simulated and experimental data of maximally 7% might result from the onset of protein layer and gas bubble formation effecting the heat transfer, which was not considered in the simulations. The slope of the temperature function in the simulation decreased from a value of 3.2 °C min^{-1} at 1 min, to a value of 1.7 °C min^{-1} at 5 min, and to a value of 0.4 °C min^{-1} at 15 min, i.e., the slope dropped by 48% at 5 min and by 89% at 15 min with respect to the value at 1 min. The current density showed an almost identical trend with the slope dropping by 50% at 5 min and by 90% at 15 min in comparison to the slope at 1 min (Fig. 4c). The electric current influences the specific energy input (Eq. (1)) and thus, higher electric currents lead to an increase in temperature and a higher temperature in turn leads to an increase in the electric current (Jaeger and Knorr, 2017). This positive feedback loop was mitigated at higher temperatures through heat dissipation by way of the large (surface to volume ratio of 2.5 cm^{-1}) thermally conductive electrodes. In contrast to the indirect conductive heat transfer, the temperatures near the electrodes were lower than in the center during μsPEF treatments, e.g., after 20 min the simulated difference in temperature was 2.2 °C (Fig. 4d).

In summary, lowering the pH increased the ion concentration, which resulted in an increase of temperature and gas formation. In addition, the pH reduction resulted in an altered overall charge of β-lg and thus to a change of the migration direction which led to the formation of protein layers on the opposite electrode. Experimental data in combination with the simulations provided valuable information on how these different domains interact with each other, what effects they trigger, how best to implement control loops, and what to consider in initial scaling up approaches.

3.2. Interplay between factor domains in the continuous setup

In a continuous setup the flow profile adds an additional layer of complexity and plays a crucial role in terms of energy input, treatment time, heat dissipation, and protein trajectories. After having applied a pulse at 2 kV cm^{-1}, 10 μs, 300 Hz for 30 min, aggregates and agglomerates were detected at the anode in a parabolic-like distribution in the x-z-plane most probably reflecting the flow profile shape (Fig. 5, Fig. S4). In the following, various potential explanations for the observed protein layer distribution are presented and discussed in more detail.

As was previously mentioned, electric fields influence the protein trajectory as a function of the electric field strength, treatment time, protein charges, mass, and the drag force (Eq. (8)). In batch, a movement in z direction was neglected during the simulation time (60 s). In the continuous setup, the average residence time was around 60 s, i.e., the movement in z-direction (along the treatment chamber length towards the outlet) is of utmost importance to gain an understanding of an

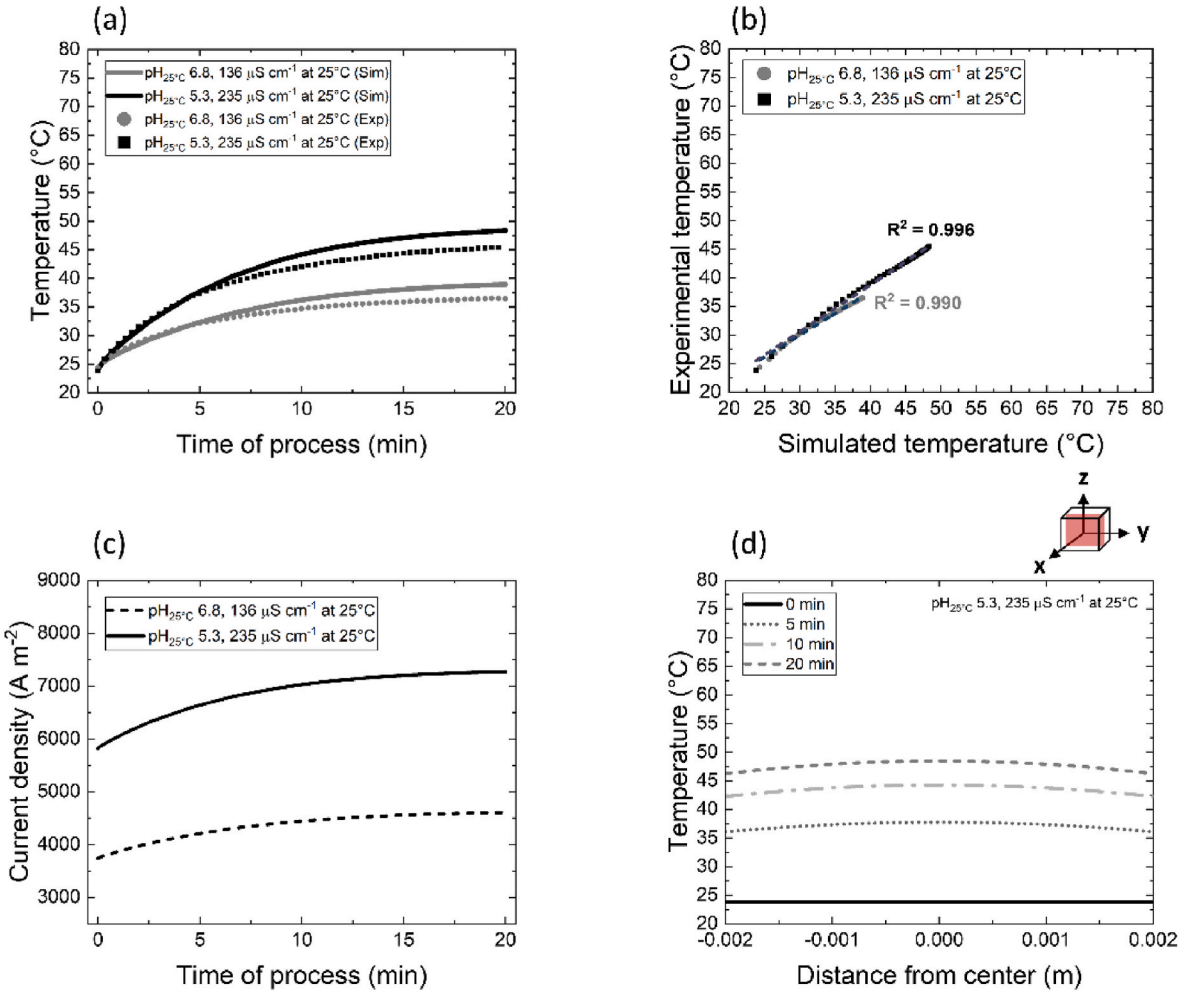

Fig. 4. (a) Simulated (Sim) and experimentally (Exp) measured time-temperature profiles resulting from PEF treatments (2.5 kV cm^{-1}, 10 μs, 40 Hz) for $pH_{25°C}$ 6.8 and 5.3 in electroporation cuvettes (0.8 mL). (b) Simulated temperature data plotted against experimental temperature values at identical points in time during 20 min with a linear fit. (c) Change of the simulated current density magnitude during the PEF treatment. (d) Temperature distribution of WPC_L at $pH_{25°C}$ 5.3 between the electrodes at 0 min, after 5 min, after 10 min, and after 20 min of applying PEF. The three-dimensional cube is intended to increase the readability and interpretation, i.e., which plane the data is plotted in.

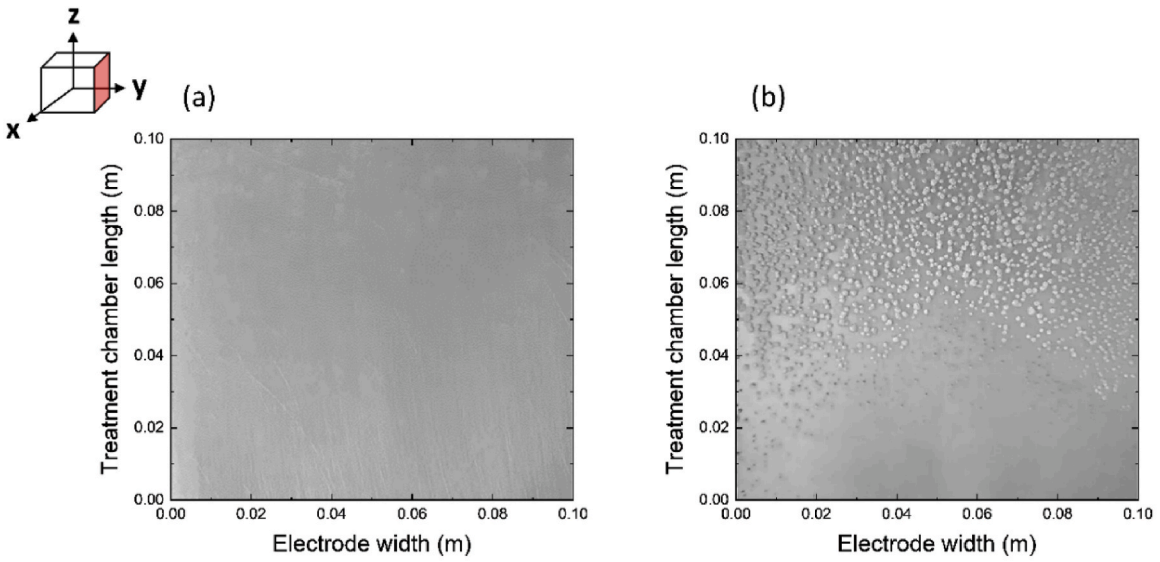

Fig. 5. Ground electrode (0.01 m^2) of the scaled up continuous system (50 mL) (a) without applying PEF and (b) after having applied 2 kV cm^{-1}, 10 μs, 300 Hz for 30 min. The diffuser inlet is located at 0.00 m, the diffuser outlet at 0.1 m, i.e., the WPC_L. The three-dimensional cube is intended to increase the readability and interpretation, i.e., which plane the data is plotted in.

idealized protein monomer trajectory. When no electric field was applied, particles followed the laminar flow profile as a function of their y-position (distance from the wall and electrode) without getting diverted (Fig. 6a). A strong electric field resulted in a migration of charged particles along the y-axis, i.e., in direction of the electrode of opposite charge. The further away these particles were from the center, the slower the movement in z-direction due to the slower velocities closer to the electrodes. At y-coordinates between −0.0025 m and 0 m, there was a positive feedback loop for the β-lg monomer (negative charge) migration, where the electric field increased the local residence time by enabling a migration towards areas of slower z-velocities (Fig. 6b). Longer residence times due to slower laminar flow velocities allowed more time for β-lg to migrate in the electric field towards areas of even slower z-velocities. Free calcium ions were expected to have an opposite trend due to their positive charge (Fig. 6c). Based on these idealized simulations a shift in β-lg and ion concentration gradients can theoretically be expected. It has been well described that β-lg transitions from an unfolding-limited to an aggregation-limited reaction at 80–85 °C and that calcium has a protective effect on β-lg unfolding (Petit et al., 2016; Tolkach and Kulozik, 2007). At temperatures ranging far below the critical threshold, as was the case in this study (Fig. 7), unfolding-limited reaction rates dominate, and these concentration gradients potentially contributed to a facilitated protein unfolding allowing hydrophobic core interactions of up-concentrated β-lg regions close to the anode.

In a multiphysics simulation approach, as was done in batch, further insights into temperature distributions were gained, and were essential to interpret the aggregation and agglomeration formation on the ground electrode. Measured time-temperature profiles agreed well with the simulations and trends based on the energy input and energy losses were

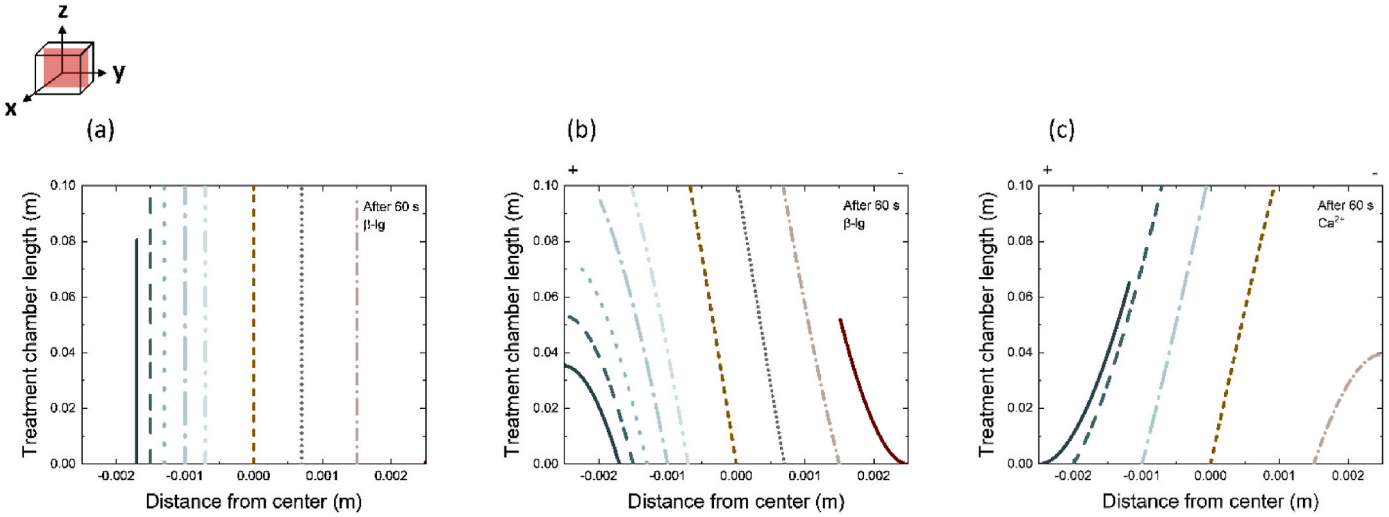

Fig. 6. Simulation of the trajectory of (a) β-lg monomers without microsecond pulsed electric field (μsPEF), (b) β-lg monomers with μsPEF and (c) calcium ions (Ca^{2+}) with μsPEF at an initial $pH_{25°C}$ of 6.8 during 60 s in the scaled up continuous system (50 mL). Simulated pulse was 2 kV cm^{-1}, 10 μs, 300 Hz. For β-lg, 9 starting coordinates were chosen ((-0.0017/0), (−0.0015/0), (−0.0013/0), (−0.001/0), (−0.0007), (0/0), (0.0007/0), (0.0015/0), (0.0025/0)). For Ca^{2+}, 5 starting coordinates ((-0.0025/0), (−0.002/0), (−0.001/0), (0/0), (0.0015/0)) were selected. Plus and minus symbols above the 1st and 2nd y-axis represent the ground and high voltage electrodes, respectively. The three-dimensional cube is intended to increase the readability and interpretation, i.e., which plane the data is plotted in.

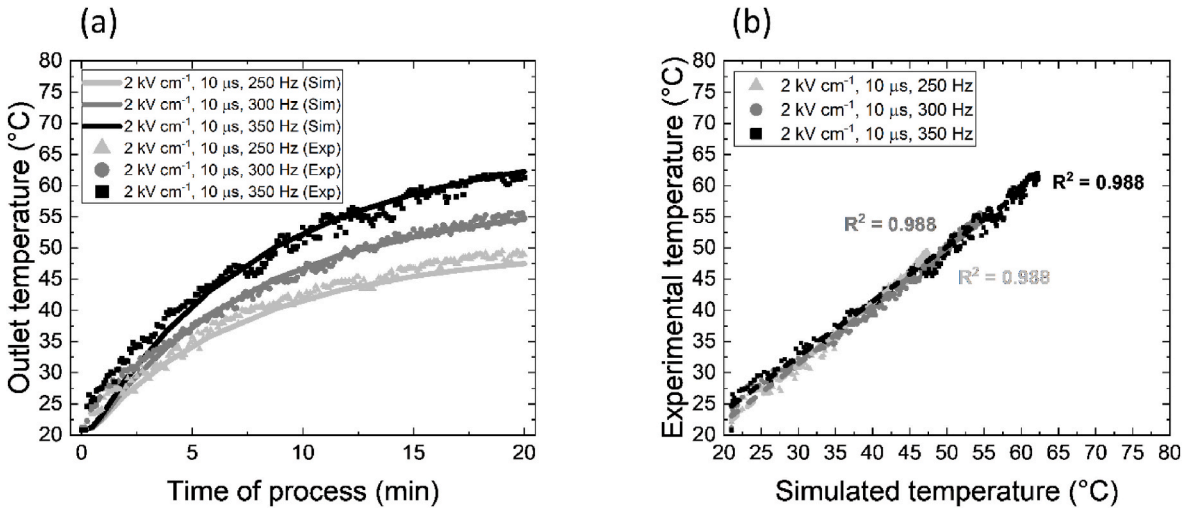

Fig. 7. (a) Simulated (Sim) and experimentally (Exp) measured time-temperature profiles resulting from PEF treatments (2 kV cm^{-1}, 10 µs, 250–350 Hz) for WPC_L at $pH_{25°C}$ 6.8 in the scaled up continuous system (50 mL). (b) Simulated temperature data plotted against experimental temperature values at identical points in time during 20 min with a linear fit.

comparable to the batch setup, despite experimental temperature fluctuations of up to 1.9 °C (Fig. 7). Different from the batch system, fluid volume elements were constantly exchanged by the inflow and outflow, thereby acting as a cooling fluid additionally contributing to heat losses in the treatment chamber. However, the surface to volume ratio in the continuous setup was smaller (2.0 cm^{-1}) in comparison to the batch setup, i.e., heat dissipated via the electrodes to the atmosphere less efficiently. The specific energy input for 250 Hz, 300 Hz, and 350 Hz during a residence time of 60 s was calculated to be 92.7 J g^{-1}, 111.3 J g^{-1}, and 129.8 J g^{-1}.

The temperature distribution across the electrode gap was decisively different at the inlet and at the outlet (Fig. 8a). At the inlet, temperatures at the electrodes were higher compared to the center by 6.2 °C after having applied a 2 kV cm^{-1}, 10 µs, 300 Hz pulse for 20 min. At the outlet, temperatures at the electrodes were lower compared to the center by 2.2 °C after 20 min. The temperature of the fluid increased with time through ohmic heating. By means of convection and conduction, heat was transferred to the electrode, which in turn heated up and dissipated some of this heat to the atmosphere. New fluid volume elements flowing into the treatment chamber got heated up in close vicinity to the electrode in addition to the ohmic heating effects. Previous work suggested that the energy input close to the wall approaches a very high value asymptotically due to a rising residence time as a function of the laminar flow (Buchmann et al., 2018). This work expands on this notion, proposing that despite a large energy input close to the wall area, the temperature is not necessarily higher than in the center. In fact, with large enough electrodes and low flow rates, the temperature in these peripheral areas can be lower than in the center. Along the treatment chamber length (z-direction), the temperature increased by 34.5 °C in the center after 20 min according to simulations (Fig. 8b). At the ground electrode the temperature increased by 26.1 °C after 20 min (Fig. S4b). The temperature increase in z-direction agreed well with observed aggregates and agglomerates on the electrode (Fig. 5b), i.e., temperatures above 40 °C lead to intramolecular transitions of β-lg unmasking the free thiol group and these temperatures were simulated at 0.05 m in z-direction (Tolkach and Kulozik, 2007). The increase in temperature additionally led to a simulated drop in viscosity, potentially resulting in a reduced residence time (Fig. 8c). However, protein layers that form might increase the viscosity and have a greater impact on the overall residence time. Continuous µsPEF treatments at 2 kV cm^{-1}, 10 µs, 300

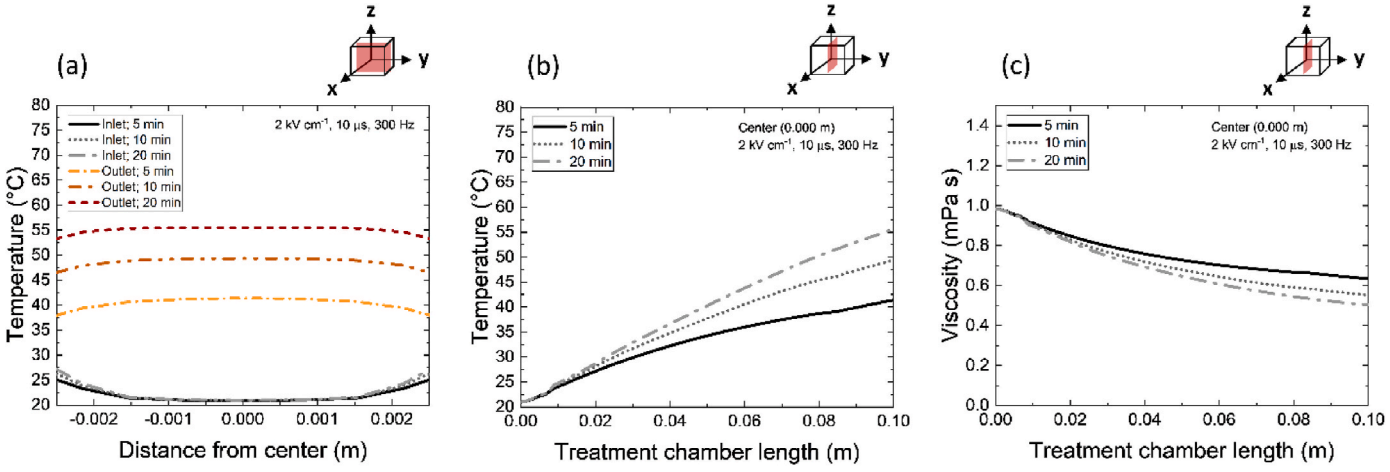

Fig. 8. (a) Simulated temperature distribution of WPC_L at the inlet and outlet between the electrodes after 5 min, after 10 min, and after 20 min of applying PEF (2 kV cm^{-1}, 10 µs, 300 Hz). (b) Simulated temperature distribution of WPC_L along the treatment chamber length in the center in between the electrodes after 5 min, after 10 min, and after 20 min of applying PEF. (c) Simulated change in viscosity along the treatment chamber length resulting from the temperature profile. Lines to guide the eye. The three-dimensional cubes are intended to increase the readability and interpretation, i.e., which plane the data is plotted in.

Hz ran smoothly for more than 1 h. It was however observed that there was an onset of electrode wear and electrochemical effects at the anode after multiple cycles. The observed protein attachment to the anode decreased from one run to the next. The importance of metal ion and metal surface interactions with whey proteins are known and have been highlighted in literature (Hedberg et al., 2013; Omanovic and Roscoe, 2000; Wagener et al., 2015). An altered composition, e.g., iron chloride and iron oxide, of the outer layers may well have led to a changed surface interaction with the whey proteins.

3.3. Interplay between factor gradients at the boundary layers

To further improve and better understand the systems in their entirety, the interaction of the overlapping factor domains based on the parameter interdependencies must be considered (Jaeger, 2012) (Fig. 9a). For example, the electric field leads to a local change of the concentration (C) e.g., local pH values or proteins, and to ohmic heating, i.e., a temperature increase. A concentration and temperature increase can lead to a change in viscosity (η) or electrical conductivity (σ), which in turn has an impact on the flow profile or on the specific energy input (W_S), respectively. The flow introduces new volume elements and partially removes the heated-up fluid (Q_{loss}). A change in the flow profile can impact the residence time (t_r) of the volume elements and the shear rate ($\dot{\gamma}$). The residence time directly impacts the exposure time of the fluid to the electrical domain, and thus can change the local temperature. Lastly, the flow profile can have an impact on the local ion or molecule concentrations.

Interacting factor domains result in local factor gradients. A local region of particular interest is the boundary layer near the anode, where protein layers formed at initial (stock WPC_L) pH values above the isoelectric point of β-lg (Fig. 9b). The protein concentration gradient is hypothesized to be of utmost importance for the observed protein interactions (Douillard, 1993; Treuheit et al., 2002). Proteins migrate from the bulk to the boundary layer increasing the protein dry weight concentration in this region to >0.4% w/w (total WPC_L dry weight = 0.5% w/w). An illustrative analogy, despite the technologies and triggering mechanisms being different, might be the concentration polarization at membrane surfaces during cross-flow filtration (Goosen et al., 2004). In near vicinity of the electrode, maximal protein concentrations are limited by steric effects, which are dependent on the pH gradient (the local pH influences the protein surface charges). Furthermore, the protein layer compression at the boundary layer induced by the migration is also dependent on the local pH. The temperature gradient leads to protein conformational changes and increases gas formation that favor protein interactions at the electrode surface and at the liquid-gas interface towards the outlet of the treatment chamber (Tolkach and Kulozik, 2007). The residence time of proteins that underwent adhesion is theoretically infinitely long, while the residence time of unattached proteins is finite (Fig. 5). Diffusion of free proteins from the boundary layer back into the bulk or creeping flow at the electrode are expected to contribute to the finite residence time. However, during the μsPEF treatment, diffusion is likely to be negligible in comparison to the migration trajectories. All factor gradients are strongly dependent on the μsPEF treatment time, i.e., how long fluid elements are exposed and influenced by the gradients.

4. Conclusions

Pulsed electric field (PEF) technology has the potential to tailor the techno-functionality of proteins by inducing structural changes. The study of effective process windows, the process stability, and scalability are therefore of great interest and importance for future industrial applications. To determine relevant PEF parameter combinations, experiments with liquid whey protein concentrate (WPC_L, 0.5% w/w) as a model fluid in combination with simulations shedding light upon the interplay of factor domains offer an effective approach. The aggregation of proteins was primarily detected at the electrode boundary layer. It is hypothesized that observed protein interactions at the boundary layer are highly dependent on the protein concentration gradient triggered by migration. Elevated temperatures, gas formation, and increased protein

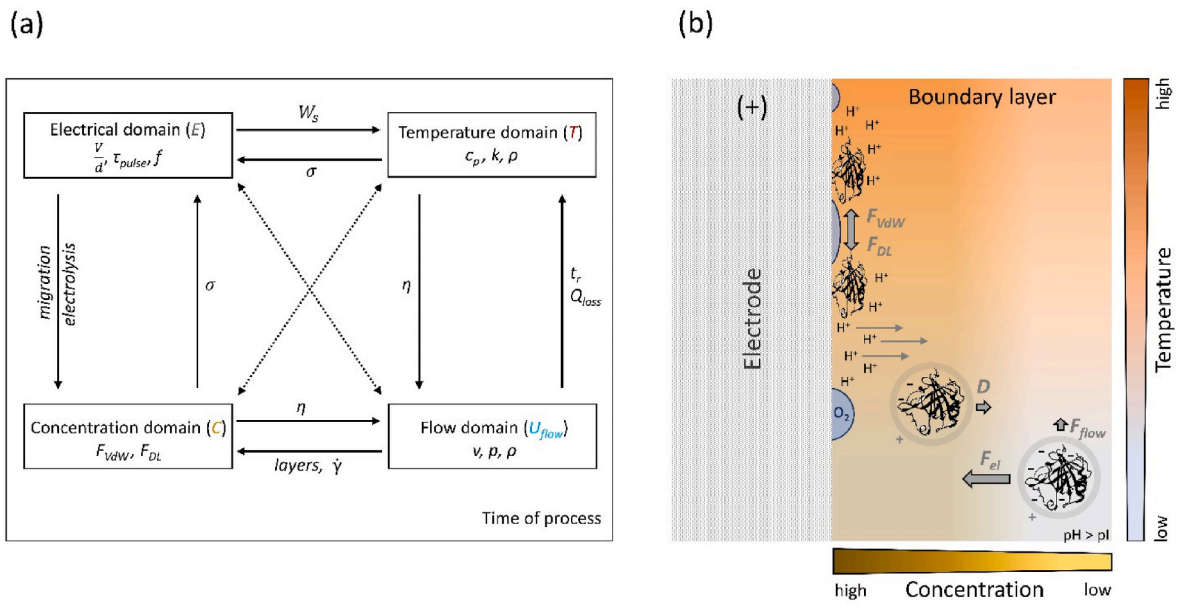

Fig. 9. (a) Interplay between different factor domains following pulsed electric field treatments. The applied voltage (V), the electrode distance (d) and geometry, the pulse length (τ_{pulse}), and the pulse repetition frequency (f) result in a pulsating electric field. The electric field leads to an interaction of the electrical domain with other domains and to various feedback loops. The interplay of the factor domains results in (b) factor gradients at the boundary layer, triggering protein interactions at the electrode and at the liquid-gas interface. The illustration is shown for an initial pH value above the isoelectric point (pI). Gray circles indicate potential charge screening of monomers. The overlaying domains and gradients additionally determine the stability of the process. Parameters: viscosity (η), electrical conductivity (σ), specific energy input (W_S), heat loss (Q_{loss}), residence time (t_r), shear rate ($\dot{\gamma}$), specific heat capacity (c_p), thermal conductivity (k), density (ρ), velocity (v), pressure (p), van der Waals forces (F_{VdW}), double layer forces (F_{DL}), electric forces (F_{el}), flow forces (F_{flow}), diffusion flux (D). Chimera package and the 1B0O protein data bank file were used for the graphical visualization of β-lg monomers (Pettersen et al., 2004; Wu et al., 1999).

residence times at the boundary layer most likely contribute to these interactions. The concept of overlapping factor domains and factor gradients offers a promising tool to characterize the interconnectivity of the entire system, allowing for a better understanding of the involved mechanisms and initial scaling up approaches. In future work, developing a dimensionless number based on the flow behavior, electrical driving force, and the involved particle properties characterizing a critical value for protein aggregation could be of great value.

Authors contributions

Robert Axelrod: Investigation, Methodology, Formal analysis, Visualization, writing original draft, Julia Baumgartner: Investigation, Methodology, Writing – review & editing, Michael Beyrer: Conceptualisation, Funding acquisition, Methodology, Data curation, Project administration, Supervision, Writing – review & editing, Alexander Mathys: Supervision, Validation, Writing – review & editing.

Declaration of competing interest

The authors have no affiliation with any organization with a direct or indirect financial interest in the subject matter discussed in the manuscript.

Data availability

Data will be made available on request.

Acknowledgements

The authors are grateful to the HES-SO VS and ETH Zurich workshops, in particular Grégory Trottet, Daniel Kiechl, Peter Bigler, and Sergio Fritz for their technical support. The authors would like to thank Dr. David Martinet and Prof. Dr. Christoph Ellert from the Institute of Sustainable Energy at the HES-SO VS, Kamran Iranshahi and Dr. Thijs Defraeye from the Laboratory for Biomimetic Membranes and Textiles at EMPA for their valuable input on multiphysics simulations. Lastly, the authors thank Etienne Tanner from ETH Zurich and Adrian Caramaschi from Hochdorf Swiss Nutrition AG for the fruitful discussions and input. This project was financially supported by the Swiss Innovation Agency (Innosuisse, Switzerland, project-nr.: 29439.1 IP-LS).

Appendix A. Supplementary data

Supplementary data to this article can be found online at https://doi.org/10.1016/j.jfoodeng.2022.111308.

References

Axelrod, R., Baumgartner, J., Tanner, E., Beyrer, M., Mathys, A., 2021. Effects of microsecond pulsed electric field (μsPEF) and modular micro reaction system (MMRS) treatments on whey protein aggregation. Int. Dairy J. 123, 105170 https://doi.org/10.1016/j.idairyj.2021.105170.

Axelrod, R., Beyrer, M., Mathys, A., 2022. Impact of the electric field intensity and treatment time on whey protein aggregate formation. J. Dairy Sci. https://doi.org/10.3168/jds.2021-21395.

Buchmann, L., Bloch, R., Mathys, A., 2018. Comprehensive pulsed electric field (PEF) system analysis for microalgae processing. Bioresour. Technol. 265, 268–274. https://doi.org/10.1016/j.biortech.2018.06.010.

Buchmann, L., Brändle, I., Haberkorn, I., Hiestand, M., Mathys, A., 2019. Bioresource Technology Pulsed electric field based cyclic protein extraction of microalgae towards closed-loop biorefinery concepts. Bioresour. Technol. 291, 121870 https://doi.org/10.1016/j.biortech.2019.121870.

Buchmann, L., Mathys, A., 2019. Perspective on pulsed electric field treatment in the bio-based industry. Front. Bioeng. Biotechnol. 7, 1–7. https://doi.org/10.3389/fbioe.2019.00265.

Buckow, R., Schroeder, S., Berres, P., Baumann, P., Knoerzer, K., 2010. Simulation and evaluation of pilot-scale pulsed electric field (PEF) processing. J. Food Eng. 101, 67–77. https://doi.org/10.1016/j.jfoodeng.2010.06.010.

Buckow, R., Semrau, J., Sui, Q., Wan, J., Knoerzer, K., 2012. Numerical evaluation of lactoperoxidase inactivation during continuous pulsed electric field processing. Biotechnol. Prog. 28, 1363–1375. https://doi.org/10.1002/btpr.1582.

Canelli, G., Kuster, I., Jaquenod, L., Buchmann, L., Murciano Martínez, P., Rohfritsch, Z., Dionisi, F., Bolten, C.J., Nanni, P., Mathys, A., 2022. Pulsed electric field treatment enhances lipid bioaccessibility while preserving oxidative stability in *Chlorella vulgaris*. Innovat. Food Sci. Emerg. Technol. 75, 102897 https://doi.org/10.1016/j.ifset.2021.102897.

Douillard, R., 1993. Applicability of polymer theories to the thermodynamics of proteins at the air/water interface: example of β-lactoglobulin. Colloids Surf. B Biointerfaces 1, 333–340. https://doi.org/10.1016/0927-7765(93)80027-V.

Engelhardt, K., Lexis, M., Gochev, G., Konnerth, C., Miller, R., Willenbacher, N., Peukert, W., Braunschweig, B., 2013. PH effects on the molecular structure of β-lactoglobulin modified air-water interfaces and its impact on foam rheology. Langmuir 29, 11646–11655. https://doi.org/10.1021/la402729g.

Fritsch, R.J., Krause, I., 2003. Electrophoresis. In: Caballero, B. (Ed.), Encyclopedia of Food Sciences and Nutrition. Elsevier, pp. 2055–2062. https://doi.org/10.1016/B0-12-227055-X/01409-7.

Gerlach, D., Alleborn, N., Baars, A., Delgado, A., Moritz, J., Knorr, D., 2008. Numerical simulations of pulsed electric fields for food preservation: a review. Innovat. Food Sci. Emerg. Technol. 9, 408–417. https://doi.org/10.1016/j.ifset.2008.02.001.

Giteru, S.G., Oey, I., Ali, M.A., 2018. Feasibility of using pulsed electric fields to modify biomacromolecules: a review. Trends Food Sci. Technol. 72, 91–113. https://doi.org/10.1016/j.tifs.2017.12.009.

Goosen, M.F.A., Sablani, S.S., Al-Hinai, H., Al-Obeidani, S., Al-Belushi, R., Jackson, D., 2004. Fouling of reverse osmosis and ultrafiltration membranes: a critical review. Separ. Sci. Technol. 39, 2261–2297. https://doi.org/10.1081/SS-120039343.

Hedberg, Y., Wang, X., Hedberg, J., Lundin, M., Blomberg, E., Odnevall Wallinder, I., 2013. Surface-protein interactions on different stainless steel grades: effects of protein adsorption, surface changes and metal release. J. Mater. Sci. Mater. Med. 24, 1015–1033. https://doi.org/10.1007/s10856-013-4859-8.

Jaeger, H., 2012. Process Performance Analysis of Pulsed Electric Field (PEF) Food Applications. TU Berlin, Germany.

Jaeger, H., Knorr, D., 2017. Pulsed Electric Fields Treatment in Food Technology: Challenges and Opportunities, Handbook of Electroporation. Springer International Publishing, Cham. https://doi.org/10.1007/978-3-319-32886-7.

Jaeger, H., Meneses, N., Knorr, D., 2009. Impact of PEF treatment inhomogeneity such as electric field distribution, flow characteristics and temperature effects on the inactivation of *E. coli* and milk alkaline phosphatase. Innovat. Food Sci. Emerg. Technol. 10, 470–480. https://doi.org/10.1016/j.ifset.2009.03.001.

Knirsch, M.C., Alves dos Santos, C., Martins de Oliveira Soares Vicent, A.A., Vessoni Penna, T.C., 2010. Ohmic heating – a review. Trends Food Sci. Technol. 21, 436–441. https://doi.org/10.1016/j.tifs.2010.06.003.

Knoerzer, K., Baumann, P., Buckow, R., 2012. An iterative modelling approach for improving the performance of a pulsed electric field (PEF) treatment chamber. Comput. Chem. Eng. 37, 48–63. https://doi.org/10.1016/j.compchemeng.2011.09.002.

Lindgren, M., Aronsson, K., Galt, S., Ohlsson, T., 2002. Simulation of the temperature increase in pulsed electric field (PEF) continuous flow treatment chambers. Innovat. Food Sci. Emerg. Technol. 3, 233–245. https://doi.org/10.1016/S1466-8564(02)00044-9.

Meneses, N., Jaeger, H., Knorr, D., 2011a. pH-changes during pulsed electric field treatments — numerical simulation and in situ impact on polyphenoloxidase inactivation. Innovat. Food Sci. Emerg. Technol. 12, 499–504. https://doi.org/10.1016/j.ifset.2011.07.001.

Meneses, N., Jaeger, H., Knorr, D., 2011b. Minimization of thermal impact by application of electrode cooling in a Co-linear PEF treatment chamber. J. Food Sci. 76, E536–E543. https://doi.org/10.1111/j.1750-3841.2011.02368.x.

Omanovic, S., Roscoe, S.G., 2000. Interfacial behavior of β-lactoglobulin at a stainless steel surface: an electrochemical impedance spectroscopy study. J. Colloid Interface Sci. 227, 452–460. https://doi.org/10.1006/jcis.2000.6913.

Pataro, G., Barca, G.M.J., Donsì, G., Ferrari, G., 2015. On the modeling of electrochemical phenomena at the electrode-solution interface in a PEF treatment chamber: methodological approach to describe the phenomenon of metal release. J. Food Eng. 165, 34–44. https://doi.org/10.1016/j.jfoodeng.2015.05.009.

Petit, J., Moreau, A., Ronse, G., Debreyne, P., Bouvier, L., Blanpain-Avet, P., Jeantet, R., Delaplace, G., 2016. Role of whey components in the kinetics and thermodynamics of β-lactoglobulin unfolding and aggregation. Food Bioprocess Technol. 9, 1367–1379. https://doi.org/10.1007/s11947-016-1726-x.

Pettersen, E.F., Goddard, T.D., Huang, C.C., Couch, G.S., Greenblatt, D.M., Meng, E.C., Ferrin, T.E., 2004. UCSF Chimera - a visualization system for exploratory research and analysis. J. Comput. Chem. 25, 1605–1612. https://doi.org/10.1002/jcc.20084.

Raso, J., Frey, W., Ferrari, G., Pataro, G., Knorr, D., Teissie, J., Miklavčič, D., 2016. Recommendations guidelines on the key information to be reported in studies of application of PEF technology in food and biotechnological processes. Innovat. Food Sci. Emerg. Technol. 37, 312–321. https://doi.org/10.1016/j.ifset.2016.08.003.

Rocha, C.M.R., Genisheva, Z., Ferreira-Santos, P., Rodrigues, R., Vicente, A.A., Teixeira, J.A., Pereira, R.N., 2018. Electric field-based technologies for valorization of bioresources. Bioresour. Technol. 254, 325–339. https://doi.org/10.1016/j.biortech.2018.01.068.

Samaranayake, C.P., Sastry, K.S., Zhang, H., 2005. E : food engineering and physical properties pulsed ohmic heating — a novel technique for minimization of electro-. Food Eng. Phys. Prop. 70.

Timmermans, R.A.H., Mastwijk, H.C., Berendsen, L.B.J.M., Nederhoff, A.L., Matser, A.M., Van Boekel, M.A.J.S., Nierop Groot, M.N., 2019. Moderate intensity Pulsed Electric

Fields (PEF) as alternative mild preservation technology for fruit juice. Int. J. Food Microbiol. 298, 63–73. https://doi.org/10.1016/j.ijfoodmicro.2019.02.015.
Tolkach, A., Kulozik, U., 2007. Reaction kinetic pathway of reversible and irreversible thermal denaturation of β-lactoglobulin. Dairy Sci. Technol. 87, 301–315. https://doi.org/10.1051/lait:2007012.
Treuheit, M.J., Kosky, A.A., Brems, D.N., 2002. Inverse relationship of protein concentration and aggregation. Pharm. Res. (N. Y.) 19, 511–516. https://doi.org/10.1023/A:1015108115452.
Wagener, V., Faltz, A.S., Killian, M.S., Schmuki, P., Virtanen, S., 2015. Protein interactions with corroding metal surfaces: comparison of Mg and Fe. Faraday Discuss 180, 347–360. https://doi.org/10.1039/c4fd00253a.
Whitney, R.M.L., Brunner, J.R., Ebner, K.E., Farrell, H.M., Josephson, R.V., Morr, C.V., Swaisgood, H.E., 1976. Nomenclature of the proteins of cow's milk: fourth revision. J. Dairy Sci. 59, 795–815. https://doi.org/10.3168/jds.S0022-0302(76)84280-4.
Wu, S.Y., Pérez, M.D., Puyol, P., Sawyer, L., 1999. β-Lactoglobulin binds palmitate within its central cavity. J. Biol. Chem. 274, 170–174. https://doi.org/10.1074/jbc.274.1.170.
Zimmermann, U., Pilwat, G., Riemann, F., 1974. Dielectric breakdown of cell membranes. Biophys. J. 14, 881–899. https://doi.org/10.1016/S0006-3495(74)85956-4.